Sensors and Materials, Vol. 8, No. 6 (1996) 389–408
MYU Tokyo

S & M 0253

Review of the Thermoelectric Efficiency of Bulk and Thin-Film Materials

Friedemann Völklein

Fachhochschule Wiesbaden
Fachbereich Physikalische Technik
Am Brückweg 26, D-65428 Rüsselsheim, Germany

(Received March 29, 1995; accepted March 18, 1996)

Key words: thermoelectric efficiency, thermoelectric sensors and generators, thermoelectric properties of bulk and thin-film materials

The thermoelectric properties of bulk and thin-film materials are reviewed. We demonstrate that the thermoelectric figure of merit z is the crucial material parameter which determines the efficiency of thermoelectric generators, coolers or sensors. Theoretical approaches for the optimization of thermoelectric materials are discussed. The most useful bulk and thin-film materials for the room, medium, and high temperature ranges and some experimental data are presented.

1. Introduction

Today a means must be found to apply the full power of modern materials science to the important problem of efficient and environmentally friendly energy conversion. Such conversion can be performed by thermoelectric devices. Their applications range from aerospace power generation to coolers and sensors. Currently, the advance of microelectromechanical systems (MEMS) is linked with the development of new thermoelectric microcomponents. Developments in materials science present a variety of new experimental techniques with the potential to crack the $z \cdot T$ barrier and to improve the parameters of thermoelectric bulk and thin-film devices.

2. Definition of the Thermoelectric Efficiency *z*

The thermoelectric efficiency (or thermoelectric figure of merit) z is the crucial material parameter for the optimization of devices for thermoelectric energy conversion (generators, coolers) and for thermoelectric sensors. Figure 1 shows a typical thermoelectric power generator.[1] Its coefficient of performance Φ (power supplied to the load/heat absorbed at hot junction) is determined by the current flow I, the load resistance R_L, the Seebeck coefficients α_n, α_p, the thermal conductance $G(\lambda_n, \lambda_p)$ and the electrical resistance $R(\rho_n, \rho_p)$ of the thermocouple and the temperatures T_H, T_C of the hot and cold junctions. Here, λ_n, λ_p are the thermal conductivities and ρ_n, ρ_p are the electrical resistivities of the individual thermoelectric legs.

$$\Phi = \frac{I^2 \cdot R_L}{(\alpha_n - \alpha_p) \cdot I \cdot T_H + G(\lambda_n, \lambda_p)(T_H - T_C) - \frac{1}{2} I^2 \cdot R(\rho_n, \rho_p)} \tag{1}$$

The maximum efficiency is[1]

$$\Phi_{max} = \frac{T_H - T_C}{T_H} \frac{\sqrt{1 + Z \cdot T} - 1}{\sqrt{1 + Z \cdot T} + T_C / T_H} \tag{2}$$

where $T = (T_H + T_C)/2$ represents the average temperature. Φ_{max} is the efficiency of an ideal reversible engine (first term) reduced by the irreversible losses of heat conduction and Joule heating in the thermocouple (second term). The second term is determined by only

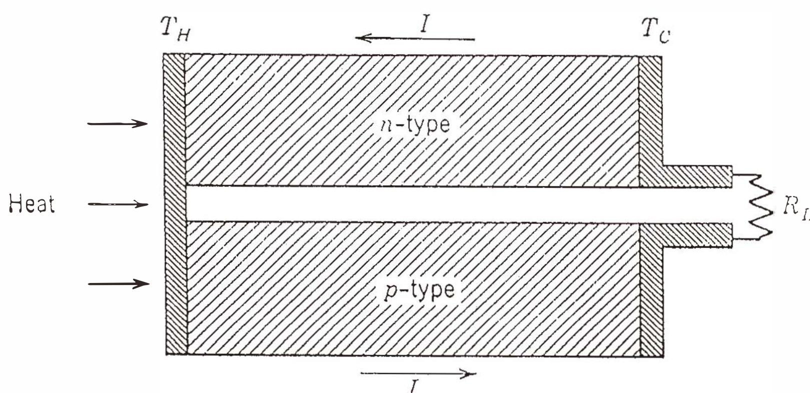

Fig. 1. Schematic of typical thermoelectric power generator. Refrigeration is achieved by replacing the resistor with a current source, and reversing the current flow.[1]

one crucial material parameter, the thermoelectric efficiency of the thermocouple Z, where

$$Z = \frac{(\alpha_n - \alpha_p)^2}{\left(\sqrt{\lambda_n \cdot \rho_n} + \sqrt{\lambda_p \cdot \rho_p}\right)^2}. \tag{3}$$

For the purpose of comparing materials it is convenient to define the figure of merit for an individual material as

$$z = \frac{\alpha^2}{\rho \cdot \lambda} = \frac{\alpha^2 \cdot \sigma}{\lambda}, \tag{4}$$

where σ is the electrical conductivity.

For thermoelectric coolers the coefficient of performance η is defined as the heat removed by the cold junction devided by power input, and it depends on the parameters and on the material properties which we also found to be significant for thermoelectric generators:

$$\eta = \frac{(\alpha_n - \alpha_p) \cdot I \cdot T_C - \frac{1}{2} I^2 \cdot R(\rho_n, \rho_p) - G(\lambda_n, \lambda_p) \cdot (T_H - T_C)}{I[I \cdot R(\rho_n, \rho_p) + (\alpha_n - \alpha_p) \cdot (T_H - T_C)]}. \tag{5}$$

The maximum efficiency is

$$\eta_{max} = \frac{T_C}{T_H - T_C} \frac{\sqrt{1 + Z \cdot T} - T_H / T_C}{\sqrt{1 + Z \cdot T} + 1}, \tag{6}$$

and the maximum temperature difference which can be achieved by the thermoelement is

$$(T_H - T_C)_{max} = \frac{1}{2} \cdot Z \cdot T_C^2. \tag{7}$$

Figure 2 demonstrates the importance of Z for the maximum temperature difference.[1] T_H is chosen as a parameter since this is usually held fixed in cooling applications.

Figure 3 represents the model of an ideal thermoelectric sensor and the corresponding heat balance.[2,3] The sensor consists of a sensitive area F (with radiation conductance G_F) coupled via two thermoelectric legs (thermal conductance G_L) to a heatsink of constant ambient temperature T_0. Without thermal input the average temperature of F is T_0, but the temperature fluctuates around this value. This fluctuation causes the "temperature noise," which ultimately limits the minimum detectable signal. When heating power N (which can

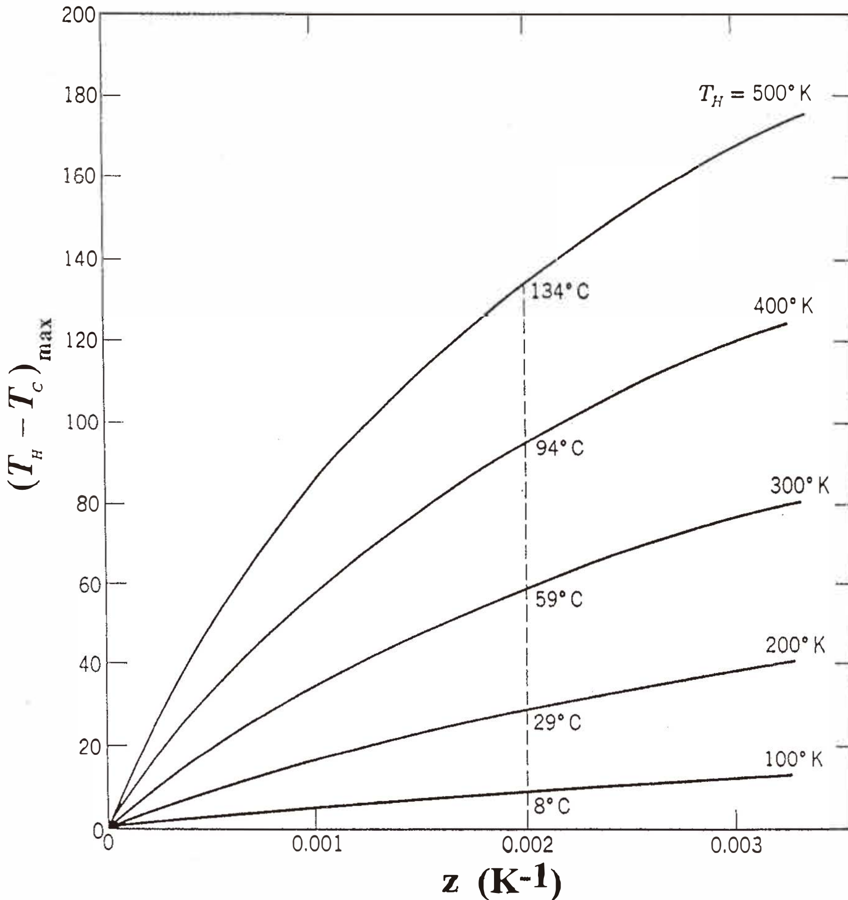

Fig. 2. Maximum temperature drop $(T_H - T_C)_{max}$ as a function of thermoelectric efficiency Z for different hot junction temperatures T_H (adapted from ref. (1)).

arise from radiation, electrical heating or other sources) is absorbed by F, the temperature increases to T_1. The heating power N is dissipated by conduction via G_L and by radiation via G_F. The corresponding heat fluxes are N_T and N_F, respectively. For small temperature differences with $(T_1 - T_0)/T_0 \ll 1$, the heat fluxes N_T and N_F can be expressed in terms of the conductances G_L and G_F. Assuming zero convection heat losses (operation in high vacuum) and negligible radiation losses of the thermoelectric legs in comparison to G_L we obtain the heat balance equation

$$N = N_T + N_F = G_L \cdot (T_1 - T_0) + G_F \cdot (T_1 - T_0), \qquad (8)$$

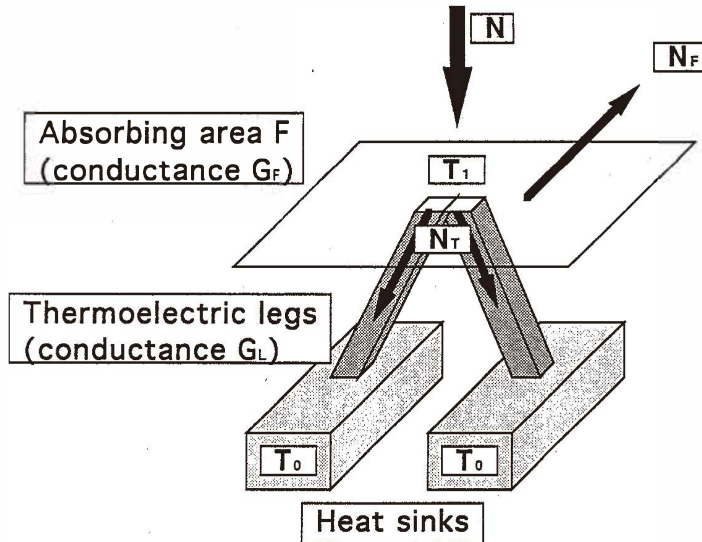

Fig. 3. Model of an ideal thermoelectric sensor.

and hence the steady state temperature increase of the sensor

$$(T_1 - T_0) = N/(G_L + G_F) = R_T \cdot N. \tag{9}$$

Here R_T denotes the thermal resistance. G_L is determined by the dimensions (length l, cross sections A_n, A_p) and the thermal conductivities of the legs, $G_L = \lambda_n A_n / l + \lambda_p A_p / l$, and G_F by the Stefan-Boltzmann law, $G_F = 4\,\varepsilon\,\sigma_s\,T_0^3\,F$, where ε denotes the emissivity of F and σ_s the Stefan-Boltzmann constant. The steady state sensitivity (responsivity) S is the ratio of the signal voltage $U = (\alpha_n - \alpha_p) \cdot (T_1 - T_0)$ to the incoming heating power N:

$$S = U/N = (\alpha_n - \alpha_p) \cdot R_T. \tag{10}$$

The noise equivalent power (NEP) relates the sensitivity S to the noise voltage U_N. For our ideal sensor we assume only thermal noise (Nyquist noise) arising from the resistance $R = l\,\rho_n / A_n + l\,\rho_p / A_p$. Hence,

$$NEP = U_N / S = \sqrt{4 \cdot k \cdot T_0 \cdot R \cdot \Delta f} \,/\, (\alpha_n - \alpha_p) R_T. \tag{11}$$

Here, Δf denotes the amplified noise bandwidth and k the Boltzmann constant. The detectivity $D = 1/NEP$ is usually referred to the sensitive area F and $\Delta f = 1$ Hz, resulting in

the specific detectivity:

$$D^* = S\sqrt{F}/U_N = (\alpha_n - \alpha_p)R_T\sqrt{F}/\sqrt{4 \cdot k \cdot T_0 \cdot R}. \quad (12)$$

The specific detectivity of our ideal sensor with a black sensitive area ($\varepsilon = 1$) reaches the maximum, when the heat flux N_T through the thermocouple legs equals the heat flux N_F radiated from the receiver area and the heat fluxes through the legs are equal. In this case the maximum detectivity is[2,3]

$$D^*_{max} = \sqrt{Z \cdot T_0}/8 \cdot \sqrt{\sigma_s \cdot k \cdot T_0^5}. \quad (13)$$

We compare eq. (13) with the general limit of the detectivity $D^*_{lim} = 1/4\sqrt{\sigma_s \cdot k \cdot T_0^5}$ for thermal sensors associated with the fluctuations of the background radiation[4,5] and find the specific detectivity of the optimized thermoelectric sensor

$$D^*_{max} = D^*_{lim}\sqrt{Z \cdot T_0}/2. \quad (14)$$

Nowadays, thermoelectric materials with $Z \cdot T_0 \approx 1$ are available. Therefore, the specific detectivity $D^*_{max} = (1/2) \cdot D^*_{lim} = 1 \cdot 10^{10}$ cm $(\text{Hz})^{1/2}$ W^{-1} seems to be the ultimate limit of the ideal thermoelectric sensor.

3. Aspects of Optimization of the Thermoelectric Figure of Merit

The Seebeck coefficient α, the electrical conductivity σ and the thermal conductivity λ are the most important transport properties characterizing thermoelectric materials. It is of interest to compare the figure of merit z for different classes of materials.[6–9]

For metals the Seebeck coefficient becomes[10]

$$\alpha = \frac{\pi^2 k^2 T}{3q}\left[\frac{\partial \ln \sigma}{\partial E}\right]_{E=E_F}, \quad (15)$$

which for monovalent metals at room temperature can be approximated[11] by $\alpha \approx \pi^2 k^2 T/qE_F$. Here, E denotes the electron energy measured relative to the Fermi energy E_F and q is the elementary charge. The thermal conductivity for metals is $\lambda = \lambda_e + \lambda_L \approx \lambda_e$ where λ_L is the lattice contribution and λ_e is the electronic contribution to the thermal conductivity. From the Wiedemann-Franz law $\lambda_e/\sigma = \pi^2 k^2 T/3q^2 = L \cdot T$ with the Lorentz number $L = 2.4 \cdot 10^{-8}$ V^2/K^2 we obtain $z = \alpha^2/LT \approx 3 \cdot 10^{-6}$ K^{-1} at $E_F = 4.4$ eV and 300 K. Thus metals are not the most desirable materials for thermoelectric devices with high efficiency.

The Seebeck coefficient for semiconductors and insulators can have much higher

values than that for metals, particularly when the Fermi level lies deep within the forbidden gap, i.e. for large $E_C - E_F$ or $E_F - E_V$, where E_C, E_V are the energies associated with the conduction and valence band edges, respectively. The limiting value of α is determined mainly by the value of the energy gap. As the Fermi level approaches midgap, contributions from charge carriers of both bands are subtractive and lower α. For this ambipolar or intrinsic conduction, the Seebeck coefficient is given by $\alpha = (\alpha_n\sigma_n + \alpha_p\sigma_p)/(\sigma_n + \sigma_p)$, where σ_n, σ_p denote the partial conductivities of the corresponding bands. High Seebeck coefficients are likely to be found in materials with large energy gap, such as insulators, where large $E_C - E_F$ or $E_F - E_V$ leads to $\alpha \approx 1$ mV/K or more. Electrical conductivities for insulators, however, are very low and lead to much smaller values of $\alpha^2\sigma$ than that of most semiconductors, as illustrated[11] by Fig. 4.

From inspection of Fig. 4 we learn that there is some optimum doping level or charge carrier concentration n_{opt} where z achieves a maximum. Therefore, in order to determine this optimum level we must relate the Seebeck coefficient and the electrical conductivity to

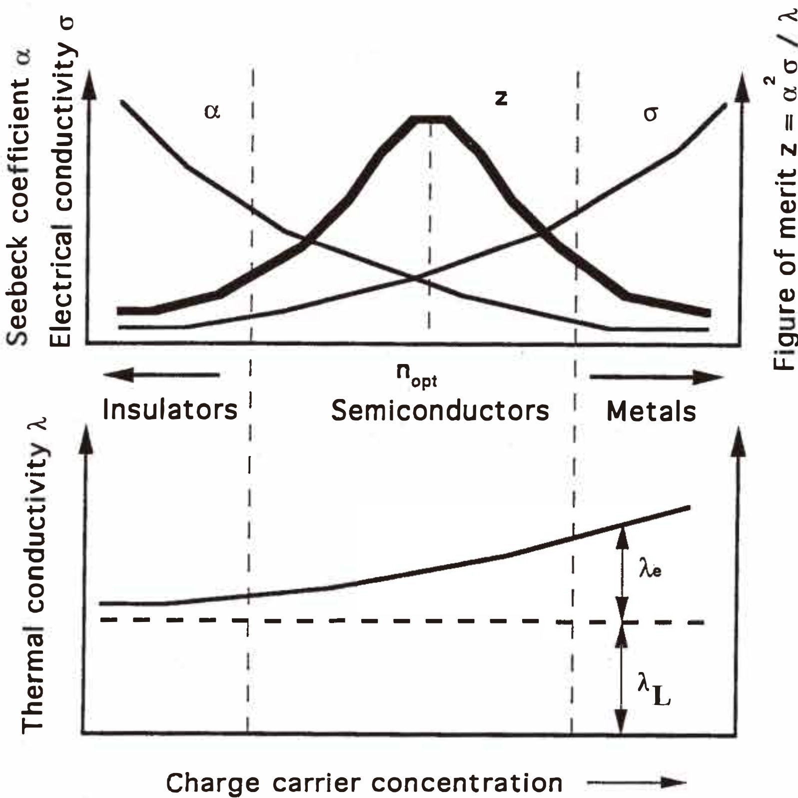

Fig. 4. Thermoelectric properties of metals, semiconductors and insulators.[11]

the charge carrier concentration. We obtain

$$\sigma = q\,\mu\,n, \tag{16}$$

$$\alpha = \pm(k/q)\cdot[\mathrm{A} + \ln(N_i/n) + \chi], \tag{17}$$

where n and μ denote the carrier concentration and mobility, respectively, N_i denotes the effective density of states in the conduction or valence band and A depends on the carrier scattering mechanism and typically ranges between 1 and 4. The positive sign holds for holes, the negative for electrons. For some semiconductors such as silicon in a certain temperature range (10 – 500 K) the phonon drag effect contributes to the Seebeck coefficient. The phonon drag contribution χ ranges from 0 for highly doped silicon to 5 for low-doped silicon at 300 K. For polysilicon films the phonon drag effect can be neglected.(12) The condition $\lambda_e \ll \lambda_L$ holds for some practical thermoelectric materials, such as silicon and the SiGe solid solutions. Under this condition and neglecting phonon drag, we maximize $\alpha^2\sigma$ from $\partial(\alpha^2\sigma)/\partial n = 0$. This leads to $\alpha_{opt} = \pm 2\cdot(k/q) = \pm 172\ \mu\mathrm{V/K}$, which is independent of temperature and scattering mechanism, and with eq. (17) yields

$$n_{opt} = N_i\cdot\exp(\mathrm{A}-2). \tag{18}$$

Assuming $N_i = 2\cdot 10^{19}\ \mathrm{cm^{-3}}$ and acoustic mode lattice scattering (A = 2) the optimum dopant level is $n_{opt} = 2\cdot 10^{19}\ \mathrm{cm^{-3}}$, and for ionized impurity scattering (A = 4) we obtain $n_{opt} = 1.48\cdot 10^{20}\ \mathrm{cm^{-3}}$. Unfortunately, these optimum carrier concentrations are too high for the original assumption of nondegenerate statistics to be valid. Therefore we must invoke the more general expressions

$$\alpha = \pm\left(\frac{k}{q}\right)\left[\frac{(r+2)F_{r+1}(\zeta)}{(r+1)F_r(\zeta)} - \zeta + \chi\right] \tag{19}$$

$$n = \frac{2}{\sqrt{\pi}}N_i\cdot F_{1/2}(\zeta) \tag{20}$$

involving the Fermi integrals

$$F_r(\zeta) = \int_0^\infty \frac{x^r}{\exp(x-\zeta)}dx, \tag{21}$$

where r characterizes the scattering mechanism (with r = 0 for acoustic mode lattice scattering and r = 2 for ionized impurity scattering) and ζ represents the reduced Fermi levels for electrons $\zeta_n = (E_F - E_C)/kT$ and for holes $\zeta_p = (E_V - E_F)/kT$. If we take into consideration the charge carrier and lattice thermal conductivities

$$\lambda = \lambda_e + \lambda_L = L(\zeta)\left(\frac{k}{q}\right)^2 \sigma \cdot T + \lambda_L \tag{22}$$

with the Lorentz number $L = L(\zeta) \cdot (k/q)^2$ and neglect phonon drag effect, the dimensionless figure of merit $z \cdot T$ can be expressed by[13]

$$z \cdot T = \frac{\left[\frac{(r+2)\ F_{r+1}(\zeta)}{(r+1)\ \ F_r(\zeta)} - \zeta\right]^2}{L(\zeta) + (r!/\beta \cdot F_r(\zeta))} \tag{23}$$

and is related to fundamental material parameters by $\beta \propto (m^*)^{3/2} \cdot \mu / \lambda_L$. Figure 5 shows $z \cdot T$ calculated according to eq. (23) as a function of the reduced Fermi level and of the parameter β. The figure of merit increases with increasing β, which suggests that the ideal thermoelectric material should satisfy the somewhat conflicting requirements of high effective mass m^*, high mobility μ, and low lattice thermal conductivity.

In conclusion, the best thermoelectric material can be achieved by an optimal doping of semiconductor alloys. The alloying of two isostructural semiconductors (such as Bi_3Te_3-Bi_2Se_3 solid solutions or SiGe alloys) introduces strong point defect scattering, which substantially lowers the lattice thermal conductivity λ_L.

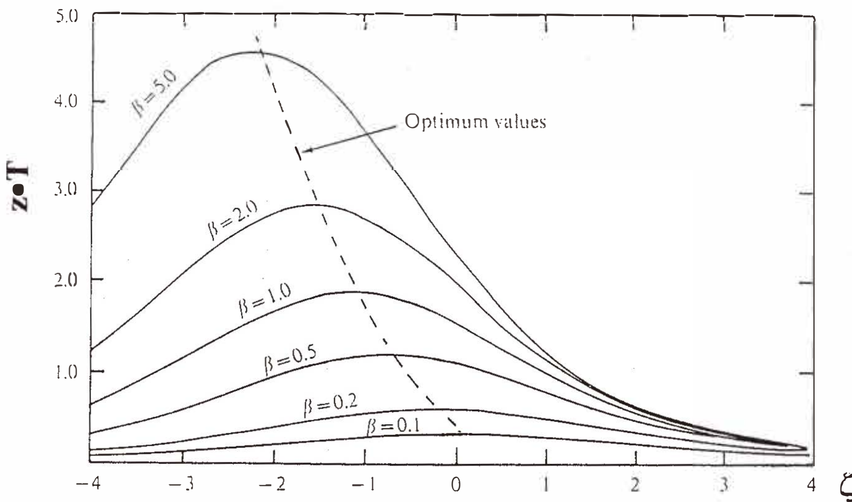

Fig. 5. Dimensionless figure of merit $z \cdot T$ as a function of the reduced Fermi level ζ for various values of the material parameter $\beta \propto (m^*)^{3/2}\ \mu / \lambda_L$ (adapted from ref. (13)).

4. Overview of Thermoelectric Bulk Materials

Figure 6 gives an overview of figures of merit for the most common thermoelectric materials at various operation temperatures. We can distinguish three groups of "conventional semiconductor materials". This term is intended to imply that the transport properties in these materials are well described by the classical semiconductor theory:

i) $(Bi_{1-x}Sb_x)_2(Te_{1-y}Se_y)_3$ solid solutions for the room (and low) temperature range(14,15)

ii) PbTe binary compounds for the medium temperature range

iii) Silicon-germanium (SiGe) alloys for high-temperature applications(16–18)

The best z values around room temperature up to $z = 3.3 \cdot 10^{-3}\ K^{-1}$ are achieved with doped solid solutions of group V-VI compounds, since the formation of solid solutions considerably reduces the lattice thermal conductivity.(19) As an example, Fig. 7 shows the thermal conductivity and figure of merit for a p-type $Bi_{0.5}Sb_{1.5}Te_3$ monocrystalline sample. It should be pointed out that the V-VI solid solutions usually show anisotropic thermoelectric properties with the best values perpendicular to the crystallographic c-axis.

Silicon-germanium alloys doped with phosphorus (for n-type materials) or boron (for p-type materials) are currently the most suitable materials for the high temperature range. Efforts to improve these materials are partly motivated by the ease with which SiGe-based

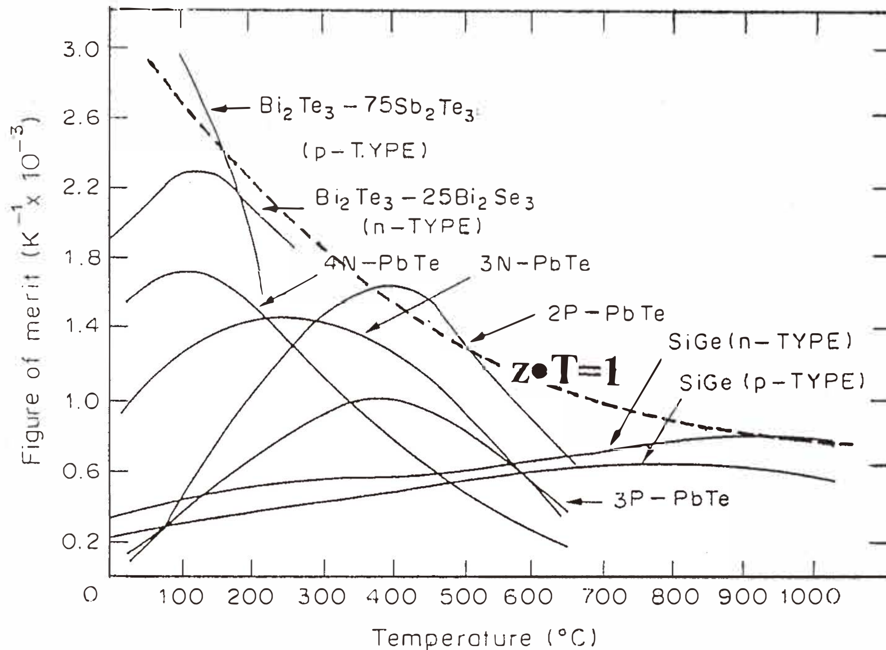

Fig. 6. Figure of merit z of selected thermoelectric materials as a function of temperature.(6) Dashed line: $z \cdot T = 1$.

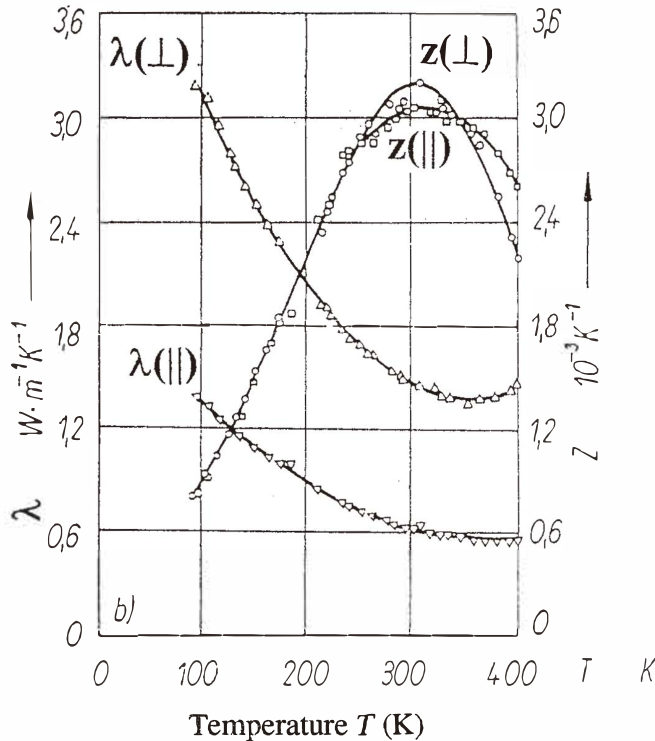

Fig. 7. Thermal conductivity λ and figure of merit z for p-$Bi_{0.5}Sb_{1.5}Te_3$ monocrystals perpendicular (⊥) and parallel (||) to the crystallographic c-axis as a function of temperature.[19]

materials advances can be translated into systems technology advances. Recently, figure of merit values which are approximately 30% higher than those for standard SiGe have been achieved in n-type SiGe alloys containing small amounts of GaP.[20]

Experimental data of the type shown in Fig. 6 appear to indicate that $z \cdot T \approx 1$ represents a limiting value. However, there is no theoretical basis for this conclusion. A number of investigators have attempted to place a theoretical upper bound on the value of $z \cdot T$ using standard semiconductor theory.[8,21–26] In fact, they found no theoretical limit. Therefore, two possibilities should be discussed:

i) $z \cdot T \gg 1$ is possible and will be demonstrated experimentally

ii) $z \cdot T \approx 1$ represents a limit due to some as yet unknown principle.

5. Thermoelectric Transport Properties of Thin Films

5.1 *Classical thin-film transport theory*

The thermoelectric properties depend on the carrier transport mechanisms. Therefore, they are modified in thin films, where the carriers are scattered by film imperfections or surface and grain boundaries. The well-known Fuchs-Sondheimer[27,28] and Mayadas-Shatzkes[29] models have been extended to thermoelectric transport.[30] According to these models, the Seebeck coefficient of polycrystalline metal films $\alpha(d,G)$ can be described by

$$\alpha_{\mathrm{bulk}} - \alpha(d,G) = \frac{\pi^2 k^2 T}{3q}\left[\frac{1}{f}\cdot\frac{\partial f}{\partial E}\right]_{E=E_F}, \tag{24}$$

where d and G denote the film thickness and average grain size, respectively. Here, f is a function of d and G, which relates the film thickness and grain size to the mean free path of the carriers. A rough approximation of f is given by

$$[f(d,G)]^{-1} \approx 1 + \frac{3(1-p_s)\gamma(E)}{8d} + \frac{3R_s\gamma(E)}{2(1-R_s)G}, \tag{25}$$

where $\gamma(E)$ denotes the mean free path and p_s, R_s denote the scattering parameters for surface and grain boundary scattering, respectively. In the framework of these models, the electrical resistivity $\rho(d,G)$ can be described by

$$\rho(d,G) = \rho_{\mathrm{bulk}}\cdot[f(d,G)]^{-1}. \tag{26}$$

For the thermal conductivity $\lambda(d,G)$, the validity of the Wiedemann-Franz law has been verified theoretically:[31]

$$\lambda(d,G)\cdot\rho(d,G) = L\cdot T. \tag{27}$$

For polycrystalline semiconductor films an extended Mayadas-Shatzkes model[32] leads to

$$\alpha(d,G) = \pm\left(\frac{k}{q}\right)\left[\frac{(r+2)}{(r+1)}\,\frac{F_{r+1}(\zeta)\cdot g_1(r,d,G)}{F_r(\zeta)\cdot g_0(r,d,G)} - \zeta\right] \tag{28}$$

$$\sigma = \sigma_{\mathrm{bulk}}\cdot g_0(r,d,G) \tag{29}$$

$$\lambda_e = L(r,d,G)\cdot T\cdot\sigma$$
$$\lambda_L = \lambda_{\mathrm{Lbulk}}\cdot g_L(d,G), \tag{30}$$

where the functions $g_m(r,d,G)$ describe the effects of thickness and grain size on α, σ and λ_e. The function $g_L(d,G)$ is deduced using a model of the phonon scattering on grain boundaries and film surfaces.[33] In many cases the ratio $g_1(r,d,G) / g_o(r,d,G)$ can be approximated by unity. Then, the partial Seebeck coefficients of the conduction or valence band equal that of the bulk material.[32] However, a distinct decrease of bulk α is observed in polycrystalline films due to suppression of phonon drag. For bipolar conduction, α can be reduced by a shift of the partial conductivities σ_n, σ_p. The influence of the various thin-film scattering mechanisms on α, σ and λ leads to a very complex variation of the thermoelectric figure of merit with film structure and temperature.

5.2 *Heterostructures*

The modern semiconductor fabrication techniques enable the preparation of materials with properties never previously achievable. Recently there have been theoretical and experimental studies of thermoelectric effects in a high-mobility two-dimensional electron gas[34] such as can be prepared in heterostructures at low temperatures. Mensah and Kangah[35] indicate that some enhancement of the Seebeck effect is expected due to the two-dimensional character of the confined carrier gas. Balmush *et al.*[36] and Dashevsky *et al.*[37] have extended the conventional description of p-n-junctions to conditions with temperature gradients and including nonlinear effects such as the Benedicks emf. Moizhes and Nemchinsky[38] have investigated the influence of energy barriers, which are placed in the current path. In this scheme α and z are improved in the direction perpendicular to the plane of the energy barriers. Hicks and Dresselhaus[39] have calculated z in one- and two-dimensional quantum well structures. They estimate that two-dimensional quantum well structures of Bi_2Te_3-based materials may have z values up to 13 times greater than those of bulk materials. Other beneficial effects are also possible with heterostructures, such as increased phonon scattering and carrier enhancement. Phonon scattering due to acoustic mismatch between layers and creation of localized modes at the interfaces are expected to contribute to reduction in phonon heat transport. As a result, flexible preparation methods such as molecular beam epitaxy (MBE) and metal-organic chemical vapor deposition are available for the fabrication of layered structures and superlattices. However, experimental attempts to apply these techniques to engineering the thermal and thermoelectric properties of thin films are still in their infancy. Theoretical investigations lead us to expect that a further increase of z by thin-film techniques can be achieved in the near future.

6. Thermoelectric Thin-Film Materials

It should be pointed out that the utility of thermoelectric thin-film materials depends not only on the thermoelectric parameters, but also on technological aspects such as: reproducible film preparation, long-term stability, simple and low-cost deposition, photolithographic patterning, adherence to substrates and compatibility with standard IC technologies. The most useful thermoelectric films for room-temperature applications are $(Bi_{1-x}Sb_x)_2(Te_{1-y}Se_y)_3$ solid solutions. They can be prepared by thermal evaporation, flash evaporation, sputtering or MBE.[40–42]

Figures 8 and 9 show the figure of merit z and the lattice thermal conductivity of $Bi_{1-x}Sb_x$ films as a function of the antimony concentration.[43] A band gap with the maximum band width at an antimony concentration of 13 at.% is induced by alloying. Therefore, the α and z values increase in comparison with those of pure bismuth[32] and antimony[44] films, which are determined by the overlap of the conduction and valence bands. Furthermore, the alloying reduces the lattice thermal conductivity by mass fluctuation scattering of phonons as demonstrated in Fig. 9.

The most efficient films at room temperature are p-$Bi_{0.5}Sb_{1.5}Te_3$ films, which are prepared by flash evaporation.[41] After deposition the thermoelectric properties must be improved by annealing as demonstrated in Fig. 10. After several hours a value $z = 2.9 \cdot 10^{-3}$ K^{-1} can be achieved, which corresponds to the best bulk values.

Lead telluride (PbTe) films[45] for the medium temperature range are normally n-type films. They can be prepared by thermal or flash evaporation. As a result of post-deposition annealing, which is necessary for an improvement of the efficiency, a z value of $0.6 \cdot 10^{-3}$ K^{-1} can be achieved at room temperature.

Metal silicides, such as CrSi films,[46] are useful materials for high-temperature applications. They can be deposited by magnetron sputtering. Their properties are strongly dependent on film structure and, consequently, on post-deposition annealing treatment, as shown in Fig. 11.

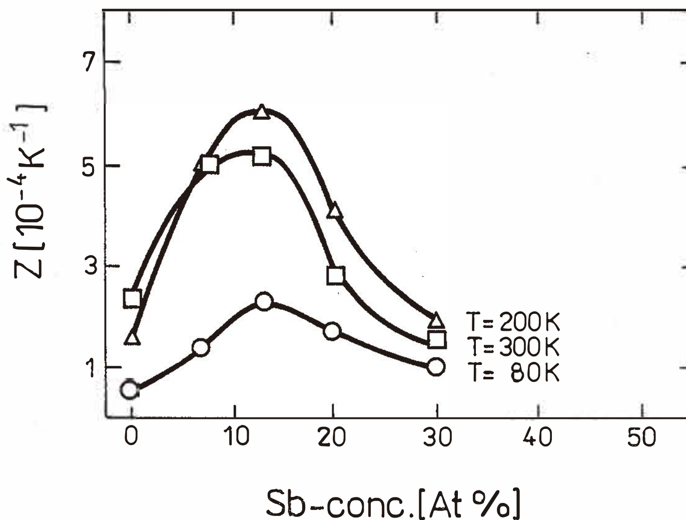

Fig. 8. Figure of merit z of $Bi_{1-x}Sb_x$ films as a function of antimony concentration.[43]

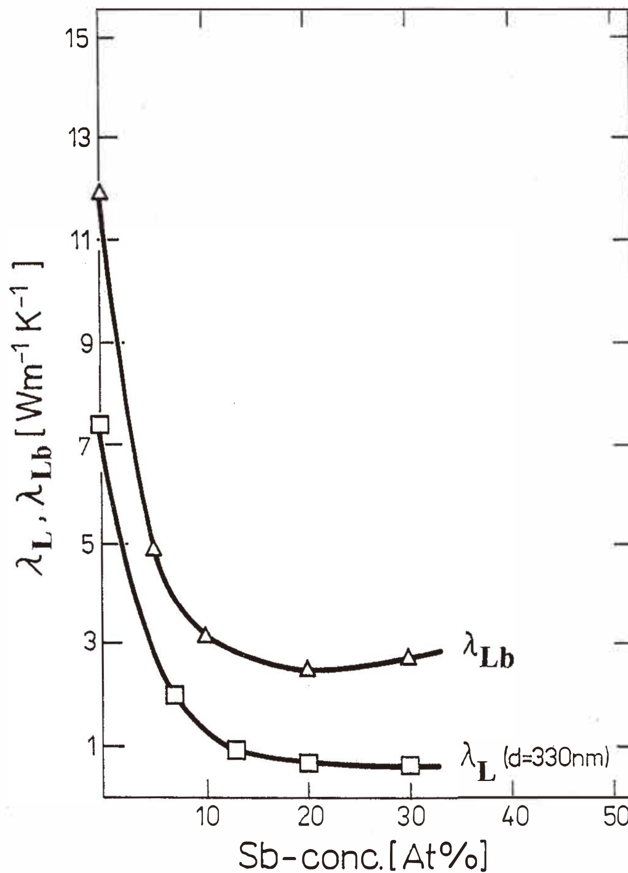

Fig. 9. Lattice thermal conductivity of $Bi_{1-x}Sb_x$ films λ_L (thickness d = 330 nm) and of the bulk λ_{Lb} vs. antimony concentration.[43]

7. Silicon and Polysilicon Films

In view of the figure of merit, silicon and polysilicon films are not the most useful materials, mainly because of their large thermal conductivity. Their z values are one or more orders of magnitude smaller than those of the best materials. However, Si and poly-Si are interesting for applications because of their well-established technology. Thermoelectric microsensors and actuators based on silicon are becoming increasingly important as components of MEMS.[2,47] The on-chip integration of such thermoelectric sensors and actuators with modern signal processing circuitries requires the use of silicon as a low-cost thermoelectric material, which is compatible with standard IC technologies. Therefore, recent investigations have been focused on the process-specific thermal and thermoelectric

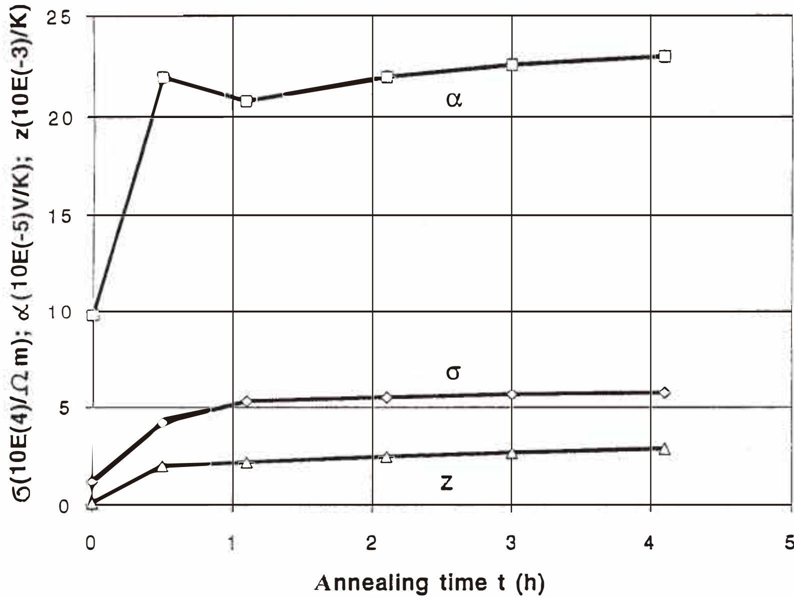

Fig. 10. Seebeck coefficient α, electrical conductivity σ and figure of merit z of p-$Bi_{0.5}Sb_{1.5}Te_3$ films as a function of annealing time for annealing in an argon atmosphere at T = 573 K.[41]

properties of Si and poly-Si films.[12,48,49]

The electrical conductivity, Seebeck coefficient and thermal conductivity of bulk Si can be described by eqs. (16), (19), and (22). These equations demonstrate that the variation of the carrier concentration by doping enables variation of α and σ over a wide range, whereas λ is dominated by the lattice component λ_L and is therefore less influenced by doping. Figure 12 shows α of bulk silicon as a function of the electrical resistivity. The Seebeck coefficient can be related to the resistivity by $\alpha = 2.6\ (k/q) \ln (\rho/\rho_o)$ with $\rho_o = 5 \cdot 10^{-6}$ Ωm (see Fig. 12).

The electrical conductivity of poly-Si films can be described by the trapping states and grain boundary scattering model.[50] Investigations of the Seebeck effect in poly-Si films[12] demonstrate that α can be interpreted using eq. (19) with a negligible phonon drag effect. Figure 13 shows α of poly-Si films, doped with boron and phosphorus, as a function of temperature. The curves are calculated according to eq. (19) with $\chi = 0$. The thermal conductivity[49] of poly-Si films is about 5 times smaller than that of the bulk because of phonon grain boundary scattering. However, we learn from Fig. 14 that λ of poly-Si films is also determined by the lattice component λ_L.

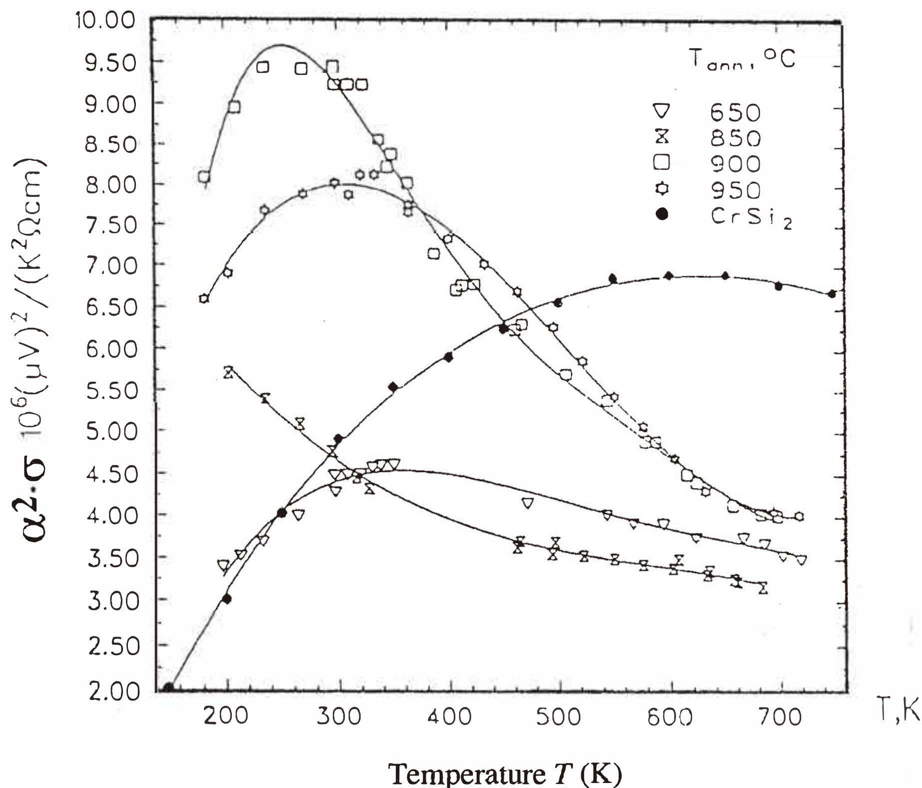

Fig. 11. Thermoelectric power factor $\alpha^2 \cdot \sigma$ of annealed $Cr_{0.22}Si_{0.78}$ films in comparison with a polycrystalline $CrSi_2$ film.[46]

8. Conclusions

It appears that, although the experimental results to date indicate that $z \cdot T \approx 1$ represents an upper limit, there is no theoretical basis for this conclusion. Modern thin-film techniques enable the preparation of layered structures on an atomic length scale with a variety of novel properties not possible with bulk materials. These techniquies may allow realization of effects beneficial to thermoelectricity such as thermal conductivity reduction and mobility enhancement. Thermoelectric thin-film sensors and actuators based on silicon, polysilicon and other materials will play an important role for MEMS, even if the thermoelectric figure of merit is not significantly increased.

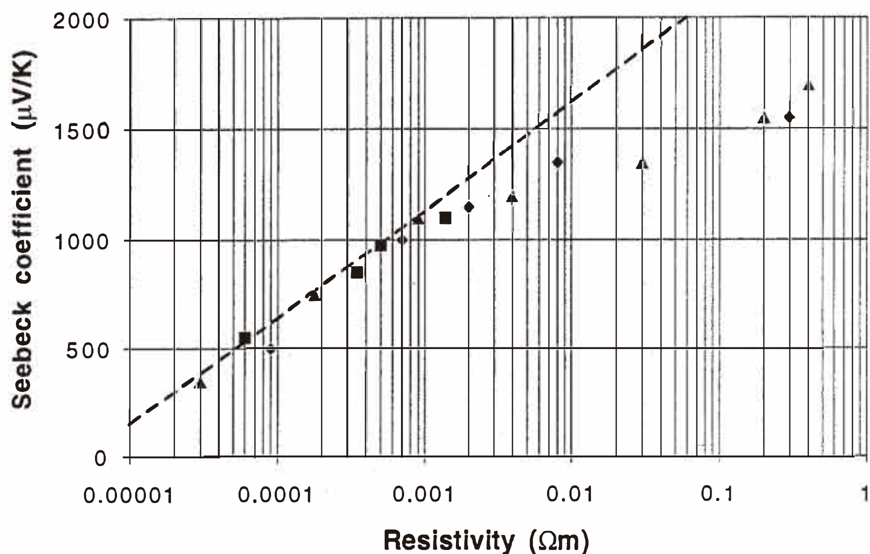

Fig. 12. Seebeck coefficient of silicon as a function of the electrical resistivity at 300 K. Symbols, experimental results; dashed line, $\alpha = 2.6\,(k/q)\ln(\rho/\rho_o)$ with $\rho_o = 5 \cdot 10^{-6}\ \Omega$m.[48]

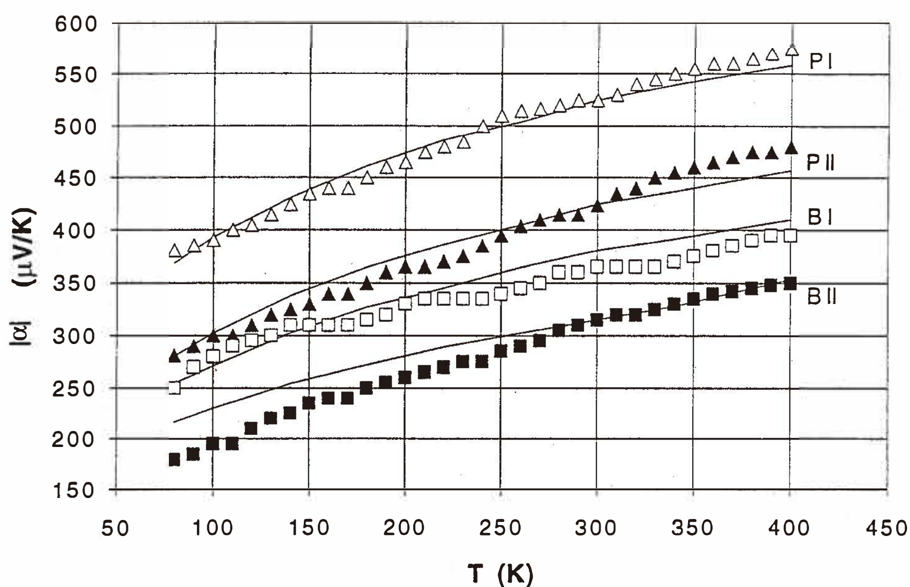

Fig. 13. Absolute value of the Seebeck coefficient α of boron- (BI and BII) and phosphorus- (PI and PII) doped polysilicon films and curves calculated from eq. (19) as a function of temperature.[12]

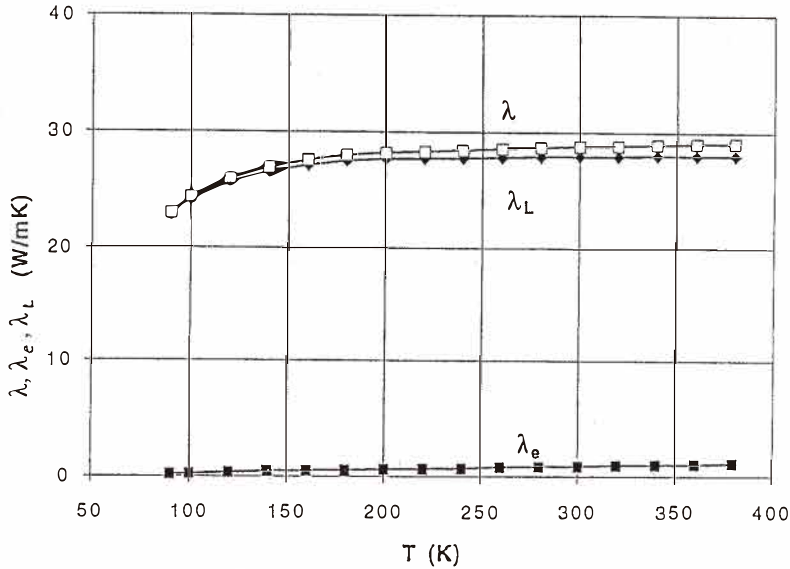

Fig. 14. Thermal conductivity λ, electron contribution λ_e, and lattice thermal conductivity λ_L of polysilicon films as a function of temperature.[49]

References

1 F. D. Rosi and E. G. Ramberg: Evaluation and Properties of Materials for Thermoelectric Applications, Thermoelectricity, ed. P. H. Egli (John Wiley & Sons, New York & London 1960) p. 121.
2 H. Baltes, D. Moser and F. Völklein: Thermoelectric Microsensors and Microsystems, Sensors—A Comprehensive Survey, Vol. 7, ed. H. H. Bau, B. Kloeck and N. F. de Rooij (VCH-Verlag, Weinheim 1993) p. 13.
3 U. Birkholz, R. Fettig and J. Rosenzweig: Sensors and Actuators **12** (1987) 179.
4 R. C. Jones: J. Opt. Soc. Am. **37** (1947) 879.
5 E. H. Putley: Thermal Detectors, Optical and Infrared Detectors, ed. R. J. Keyes (Springer, Berlin 1977) p. 71.
6 C. Wood: Energy Convers. Mgmt. **24** (1984) 317.
7 C. Wood: Reports on Progress in Physics, **51** (1988) 459.
8 C. B. Vining: Proc. XIth Int. Conf. on Thermoelectrics (Arlington 1992) p. 276.
9 C. B. Vining: Proc. XIIth Int. Conf. on Thermoelectrics (Yokohama 1993) p. 37.
10 H. Fritsche: Solid State Comm. **9** (1971) 1813.
11 A. F. Joffe: Semiconductor Thermoelements and Thermoelectric Cooling (Infosearch, London 1957).
12 F. Völklein and H. Baltes: Sensors and Materials **3** (1992) 325.
13 D. M. Rowe and C. M. Bhandari: Modern Thermoelectrics (Holt, Rinehart and Winston, London 1983) Chap. 3.
14 J. P. Fleurial: Proc. XIth Int. Conf. on Thermoelectrics (Arlington 1992) p. 270.